= ATOMS, MOLECULES, OPTICS =

DYNAMICS OF COHERENT ATOMIC WAVES DURING LIGHT SCATTERING ON A DILUTE GAS BEC

© 2024 Yu. A. Avetisyan^{a*} and E. D. Trifonov^{b**}

^aInstitute of Precision Mechanics and Control Problems, Saratov Federal Research Center RAS, Saratov, 410028 Russia ^bGertsen State Pedagogical University of Russia, St. Petersburg, 191186 Russia

> *e-mail: yuaavetisyan@mail.ru **e-mail: thphys@herzen.spb.ru

> > Received April 03, 2024 Revised June 26, 2024 Accepted June 28, 2024

Abstract. Generation and evolution of coherent atomic waves induced by superradiant light scattering on a Bose-Einstein condensate of dilute gas in a harmonic trap are theoretically analyzed

The article is presented within the framework of the conference proceedings "Physics of Ultracold Atoms" (PUCA-2023), Novosibirsk, December 2023.

DOI: 10.31857/S004445102410e067

1. INTRODUCTION

We consider light scattering on a Bose-Einstein condensate (BEC) of a dilute gas [1–14]. In particular, in the experiment [4], the BEC was irradiated by a pair of counter-propagating laser pulses traveling in a direction perpendicular to the elongation axis of the sample. As a result of multiple interactions with radiation, BEC atoms acquired corresponding translational motion momentums, close in magnitude to a series of values $j\hbar k_0$ ($j = \pm 2, \pm 4,...$), where k_0 is the absolute value of the optical pumping field wave vector. This led to the appearance of a series of coherent atomic clouds moving in opposite directions. In this work, we present the results of a theoretical analysis of their translational motion, refining our previously obtained results [15–22]. In particular, attention is drawn to the influence of the harmonic form of the trap potential on the process dynamics. If BEC is trapped in a harmonic trap, its atoms should be in the ground state of the harmonic oscillator. As a result of light scattering, the atom receives a recoil momentum and therefore ends up in the ground state with a shifted momentum. It is well known that such a state in quantum optics is interpreted as a quantum coherent state and is

widely used in laser theory [23]. In our case, we are dealing with coherent states of the atomic system rather than with coherent states of the quantized electromagnetic field. The development of methods for generating coherent atomic waves ("atomic laser") is relevant in the field of atomic interferometry and laser manipulation of atoms.

2. BASIC EQUATIONS

We model a condensate atom as a two-level boson particle with the ground $|a\rangle$ and excited $|b\rangle$ electronic states, taking into account the translational motion of the atom along the direction of optical excitation. The single-atom wave function is sought in the form Одноатомная волновая функция аndщется в виде

$$\Psi(x,t) = \sum_{j=0,\pm 2,\dots} \{a_j(x,t)e^{ijk_0x}a + e^{-i\omega_0t}b_{j+1}(x,t)e^{i(j+1)k_0x}b\},$$
(1)

where x is the coordinate of the atom's translational motion, ω_0 and $k_0 = \omega_0 / c$ are the frequency and

wave vector of the exciting laser field, $a_j(x,t)$, $b_j(x,t)$ are the amplitudes of the wave functions describing the translational motion of the atom in the ground and excited atomic states.

The Maxwell-Schrödinger system of equations in the approximation of slow variation of field amplitudes and atomic wave functions has the form

$$\left(\frac{\partial}{\partial t} + \mathbf{v}_{j} \frac{\partial}{\partial x}\right) a_{j} = \\
= -i\varepsilon_{j} a_{j} + E^{+} b_{j+1} + E^{-} b_{j-1} - iux^{2}, \\
\left(\frac{\partial}{\partial t} + \mathbf{v}_{j+1} \frac{\partial}{\partial x}\right) b_{j+1} = \\
= i \left(\Delta - \varepsilon_{j+1} + i\frac{\gamma}{2}\right) b_{j+1} - \\
-E^{+} a_{j} - E^{-} a_{j+2} - iux^{2}, \\
E^{+}(x,t) = \\
= E_{0}(t) + 2 \int_{-\infty}^{x} dx' \sum_{j=0,\pm2,\dots} b_{j+1}(x',t) \overline{a}_{j}(x',t),$$
(2)

The only non-zero initial condition was set for $a_0(x,t)$ as the wave function of the ground state of a harmonic oscillator.

Equations (1), (2) are written in the dimensionless form, where the "width" of the ground state of the harmonic oscillator is taken as the unit of length,

$$L = 2(\hbar \ln 2 / M\Omega)^{1/2},$$

where M and Ω are the atomic mass and natural frequency of the harmonic trap, respectively. The superradiance time is taken as the unit of time

$$\tau_R \equiv \hbar / (\pi d_{ab}^2 k_0 N_0 L),$$

where d_{ab} is the dipole moment of the transition $a \leftrightarrow b$ and N_0 is the average concentration of BEC atoms at the initial instant. Further,

$$\varepsilon_{j} = \hbar j^{2} k_{0}^{2} \tau_{R} / (2M),$$

$$v_{j} = \hbar j k_{0} \tau_{R} / (ML)$$

are, respectively, the kinetic energy (in frequency units) and velocity of an atom with the momentum

 jk_0 , the index j takes even values $0,\pm 2,\pm 4,...$, field strength amplitudes E_0 , E^\pm are expressed in units of $i\hbar/(d_{ab}\tau_R)$,

$$u = 0.5M\tau_R(\Omega L)^2 / \hbar$$

is the harmonic trap constant,

$$\Delta = (\omega_0 - \omega_{ab})\tau_R$$

is the detuning of the excitation field frequency ω_0 from the atomic resonance frequency ω_{ab} ,

$$\gamma = \Gamma \tau_R$$

where Γ is the radiation constant of the excited electronic state of the atom.

3. SIMULATION RESULTS

Below are the results of solving system of equations (2) obtained using atomic system parameters of the same order as in the experiment [4], but as applied to our magnetic trap model. A harmonic with the natural frequency Ω / 2π = 14 Hz was considered, which leads to a "width" of the harmonic oscillator ground state of $L\approx 4.8~\mu m$. With a transition dipole moment of $d_{ab}=2.5\cdot 10^{-29}~{\rm C\cdot m}$, pumping field wavelength of 780 nm, and initial average BEC atom density of $N_0=10^{13}~{\rm cm}^{-3}$ the superradiant time is estimated as $\tau_R\approx 15~{\rm ns}$. Taking the spontaneous decay constant of the excited electronic state of the atom as $\Gamma=0.37\cdot 10^8~{\rm s}^{-1}$, atom mass as $M=1.44\cdot 10^{-25}~{\rm kg}$, for the parameter values in Eqs. (2), we approximately obtain

$$\varepsilon_j = 3.6 \cdot 10^{-4} j^2, \quad v_j = 1.9 \cdot 10^{-5} j,$$

$$\gamma = 5.7 \cdot 10^{-1}, \quad u = 1.84 \cdot 10^{-6}.$$

In our calculations, the detuning from the resonant transition Δ varied in the interval $-100\,\mathrm{MHz} \le \Delta / 2\pi \le 100\,\mathrm{MHz}$ (in our units $-9.5 \le \Delta_{ab} \le 9.5$). The condensate excitation was modeled by two counter-propagating rectangular laser pulses with the duration $t_p \approx 6\,\mathrm{ms}$ (in our units $t_p \approx 400$). The pumping amplitude E_0 was chosen (depending on the detuning from the resonance) such that during the excitation time, the fraction of atoms in the static condensate cloud remained at the level of 0.9. The system of equations was solved

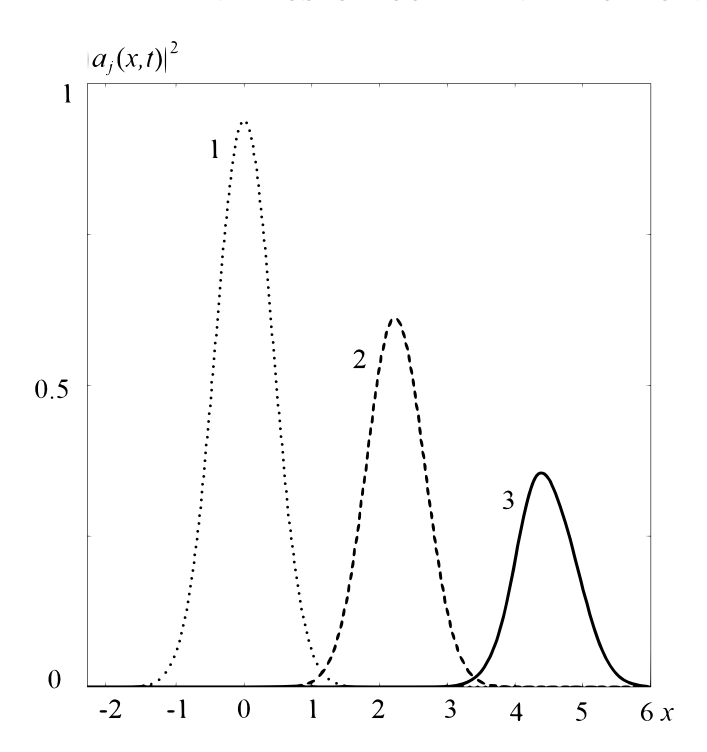


Fig. 1. Spatial distributions of atomic cloud populations: curve *I* shows the initial population distribution of the BEC ground cloud $|a_0(x,t=0)|^2$, curve *2* shows the population distribution of cloud $|a_2(x,t)|^2 \cdot 50$, and curve *3* shows the cloud $|a_4(x,t)|^2 \cdot 10^4$ at the instant $t=150t_p$

taking into account the formation of 15 atomic states $(j = 0,\pm 1,\pm 2,\pm 3,\pm 4,\pm 5,\pm 6,\pm 7)$. The calculation interval length was twelve times greater than the "width" of the harmonic oscillator ground state, taken as the unit of length.

We will limit ourselves here to presenting results obtained at detuning $\Delta / 2\pi = -20$ MHz (in our units approximately -1.9) for atomic states $a_{\pm 2}$, $a_{\pm 4}$. (Populations of states a_j at |j| > 4 are negligibly small).

The displacement of the maximum of atomic cloud distributions over time is caused by the atom acquiring photon recoil momentum. The distributions for clouds with negative indices have symmetric displacements in the opposite direction. Meanwhile, the shape of atomic clouds is approximately preserved and close to the shape of the harmonic oscillator ground state (see Fig. 1). The velocity of the cloud maximum displacement a_2 approximately corresponds to the photon recoil estimate $2\hbar k_0$.

Momentum distributions $f_j(k,t)$ of the states a_j , obtained using Fourier transformation of the corresponding amplitudes,

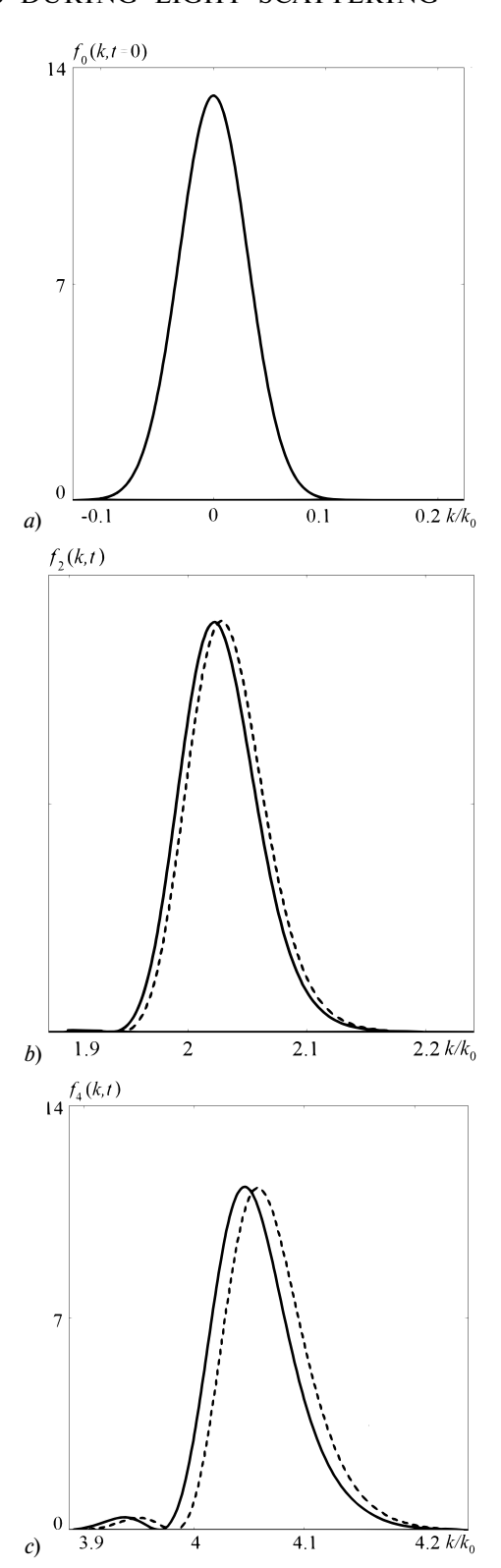


Fig. 2. Momentum (normalized) distributions of atomic clouds $(a)-f_0(x,t=0)$, initial momentum distribution of the main cloud a_0 ; $(b)-f_2(k,t)$, momentum distribution of the cloud a_2 ; $(c)-f_4(k,t)$, momentum distribution of the cloud a_4 . In fragments (b) and (c), dashed curves demonstrate momentum distributions at the instant $t=t_p$ of pumping shutdown, and solid curves are for the instant $t=150t_p$

$$f_j(k,t) = |\tilde{a}_j(k-jk_0,t)|^2,$$
 (3)

where

$$\tilde{a}_{j}(k,t) = \int_{-\infty}^{+\infty} dx a_{j}(x,t) \exp(-ikx), \tag{4}$$

are shown in Fig. 2.

The found momentum distributions demonstrate, firstly, an increase in the recoil momentum due to medium dispersion, i.e., the influence of the secondary atomic field created by their polarization on the scattering process, and secondly, a decrease in the obtained recoil momentum during subsequent movement of atomic clouds in the potential field of the harmonic trap.

4. CONCLUSIONS

Thus, based on the solution of the proposed Maxwell-Schrödinger system of equations, the generation of coherent atomic waves resulting from light scattering by a Bose-Einstein condensate of dilute gas confined in a harmonic trap is theoretically analyzed.

Our results allow us to conclude that atomic clouds arising from light scattering on BEC in a harmonic trap after pumping termination are close to the oscillator ground state with a momentum value shifted by the recoil momentum value. This allows us to consider them as an analog of Glauber quantum optical coherent states [23].

FUNDING

The work of Yu.A.A. was carried out within the state assignment of the Ministry of Education and Science of Russia (topic No. 121022000123-8).

REFERENCES

1. S. Inouye, A. P. Chikkatur, D. M. Stamper-Kurn et al., Science **285**, 571 (1999).

- S. Inouye, R. F. Löw, S. Gupta et al., Phys. Rev. Lett. 85, 4225 (2000).
- 3. D. Schneble, Y. Torii, M. Boyd et al., Science **300**, 475 (2003).
- **4.** G. K. Campbell, A. E. Leanhardt, J. Mun et al., Phys. Rev. Lett. **94**, 170403 (2005).
- L. Deng, E. W. Hagley, Q. Cao et al., Phys. Rev. Lett. 105, 220404 (2010).
- 6. N. S. Kampel, A. Griesmaier, and M. P. Hornbak Steenstrup, Phys. Rev. Lett. **108**, 090401 (2012).
- 7. I. Dimitrova, W. Lunden, J. Amato-Grill et al., Phys. Rev. A **96**, 051603 (2017).
- **8.** M. G. Moore and P. Meystre, Phys. Rev. Lett. **83**, 5202 (1999).
- Ö. E. Müstecaplioglu and L. You, Phys. Rev. A, 62, 063615 (2000).
- **10**. G. R. M. Robb, N. Piovella, and R. Bonifacio, J. Opt. B **7**, 93 (2005).
- 11. O. Zobay, Las. Phys. 19, 700 (2009).
- **12**. C. J. Zhu, L. Deng, E. W. Hagley et al., Laser Phys. **24**, 065402 (2014).
- **13**. R. Ayllon, J. T. Mendon?a, A. T. Gisbert, et al., Phys. Rev. A **100**, 023630 (2019).
- **14**. V. B. Bobrov and S. A. Trigger, J. of Low Temperature Phys. **200**, 118 (2020).
- 15. E. D. Trifonov, JETP 120, 1117 (2001).
- **16**. Yu. A. Avetisyan and E. D. Trifonov, Las. Phys. Lett. **1**, 373 (2004).
- **17**. Yu. A. Avetisyan, E. D. Trifonov, JETP **130**, 771 (2006).
- **18**. Yu. A. Avetisyan, E. D. Trifonov, Opt. and Spectr. **105**, 613 (2008).
- **19**. Yu. A Avetisyan and E. D. Trifonov, Phys. Rev. A **88**, 025601 (2013).
- **20**. Yu. A. Avetisyan, E. D. Trifonov, Phys. Usp. **185**, 307 (2015).
- **21**. Yu. A. Avetisyan, V. A. Malyshev, and E. D. Trifonov, J. Phys. B: At. Mol. Opt. Phys. **50**, 085002 (2017).
- **22**. Yu. A. Avetisyan, V. A. Malyshev, E. D. Trifonov, JETP **157**, 454 (2020).
- **23**. R. Glauber, *Optical Coherence and Photon Statistics*, Mir, Moscow (1966).

= ATOMS, MOLECULES, OPTICS =

MAGNETO-OPTICAL TRAPS FOR POTASSIUM-39 AND POTASSIUM-40

© 2024 V. V. Baturo^a, V. A. Vinogradov^{a,b,c}, M. V. Platonova^{a,b,d}, I. V. Yukhnovets^{a,c}, and A. V. Turlapov^{a,b,c,*}

^aInternational Center for Quantum Optics and Quantum Technologies LLC, Moscow, 121205 Russia ^bGaponov-Grekhov Institute of Applied Physics of the Russian Academy of Sciences, Nizhnv Novgorod, 603155 Russia

^cMoscow Institute of Physics and Technology, Dolgoprudny, Moscow Region, 141701 Russia ^dLobachevsky State University of Nizhny Novgorod, Nizhny Novgorod, 603022 Russia

*e-mail: turlapov@appl.sci-nnov.ru

Received April 03, 2024 Revised May 31, 2024 Accepted May 31, 2024

Abstract. Magneto-optical traps are created for ^{39}K and ^{40}K . The same setup can be tuned to trap either one isotope or the other. Trapped $7 \cdot 10^9$ atoms ^{39}K and $1.5 \cdot 10^8$ atoms ^{40}K . Among traps filled from a Zeeman slower, these values are the highest for each isotope. For ^{40}K , the influence of collisions with thermal beam atoms on the accumulation time is studied for the first time. Thermometry performed with fewer atoms showed 4.5 mK for ^{39}K and significantly less for ^{40}K , 130 μK , which is below the Letokhov-Minogin-Pavlik limit.

The article is presented as part of the conference proceedings "Physics of Ultracold Atoms" (PUCA-2023), Novosibirsk, December 2023.

DOI: 10.31857/S004445102410e079

1. INTRODUCTION

Laser cooling and trapping of atomic gas [1] creates conditions for subsequent deeper cooling to quantum degeneracy [2]. Laser cooling works most simply for alkali metals, which include potassium. It has two stable bosonic isotopes ³⁹K and ⁴¹K and a fermionic isotope ⁴⁰K with a long half-life of 10⁹ years.

Boson ³⁹K possesses broad *s*-wave Fano-Feshbach resonances in magnetic fields lower than for other alkali metals [3]. This opens up the possibility of faster control of *s*-interactions, which is interesting for interferometry on squeezed states of Bosecondensate [4] and for studying dynamic effects.

⁴⁰K along with ⁶Li is one of two long-lived fermionic isotopes of alkali metals, and its *s*-wave Feshbach resonances occur at significantly lower magnetic fields than those of ⁶Li. Due to a lower

centrifugal barrier than that of lithium, the p-resonances for 40 K are broader, which is interesting in the context of obtaining superfluid phases with p-symmetry [5]. Natural potassium contains only 0.012% 40 K, which complicates experiments.

Bose and Fermi gases with large numbers of the particles N are interesting. In measurements, this allows improving the signal-to-noise ratio. For collective effects, temperature in natural energy units is important, for example, in units of chemical potential μ . The minimum achievable temperature for uniform Bose and Fermi gases, respectively, scales as $\mu N^{-7/15}$ and $\mu N^{-1/3}$ [6].

A magneto-optical trap (MOT) can be loaded with atoms from a decelerated thermal beam [7], surrounding vapors [8], or a two-dimensional MOT [9]. When loading from surrounding vapors, the number of atoms advantageously depends on the MOT beam diameter d as $(N \propto d^{5.82})$, which allows

486 BATURO et al.

obtaining up to $N = 1.4 \cdot 10^{11}$, as shown for ⁸⁷Rb [10]. Such favorable scaling requires vapor pressures much higher than the pressure of other gases in the vacuum chamber. Using a slow atom beam obtained with a Zeeman slower or two-dimensional MOT allows the use of vacuum chambers with low pressure and thus long accumulation of atomic gas in the trap, avoiding losses caused by collisions with the background gas. Low pressure allows subsequent operations, such as evaporative cooling [2], in the same vacuum chamber without transfering to a chamber with lower pressure. For Na, two loading methods are compared, through a decelerator and from a two-dimensional MOT, showing that the decelerator yields slightly more atoms [11].

The implementation of all three MOT loading methods is described, respectively, in [12–14] for 39 K, and in [15–17] for 40 K. For both isotopes, the largest number of atoms was obtained by loading from a 2D MOT, (2–3) $\cdot 10^{10}$ [18, 19] and $8.9 \cdot 10^{9}$ [20] respectively. This method is mentioned most frequently in publications. Loading from surrounding vapors yielded $3 \cdot 10^{9}$ atoms for 39 K [21] and $2 \cdot 10^{8}$ for 40 K with a vapor source enriched to 4.5% in 40 K [22].

A decelerator was used for loading 39 K in two works, where $3 \cdot 10^7$ [12] and 10^8 atoms [23] were obtained in MOT. In the latter case, the atomic beam is created by a pulsed source in which 39 K vapors are pre-cooled by cold helium buffer gas, and MOT loading occurs rapidly within 10 ms. For 40 K two experiments on MOT loading from a decelerator are also known. In [15] more than 10^6 atoms were trapped from an enriched mixture containing 40 K 7% while the 40 K beam was combined with an atomic beam of 6 Li. In [24] $5 \cdot 10^7$ atoms were loaded

into MOT from a natural potassium mixture. Thus, the decelerator is not a frequently used method for MOT loading for either ³⁹K, or ⁴⁰K.

This work reports on obtaining magneto-optical traps for 39 K and 40 K loaded from a Zeeman decelerator. The number of 39 K atoms in the trap, $7 \cdot 10^9$, is larger than in other experiments with 39 K, loaded from a decelerator. 40 K trap captured $1.5 \cdot 10^8$ particles, which is also more than in other traps for 40 K, using a decelerator. For 40 K the influence of collisions with beam atoms on accumulation time was studied for the first time. The article is structured as follows. Section 2 describes the experimental setup, and Section 3 presents and discusses measurements of atom numbers, temperature, and accumulation time.

2. EXPERIMENTAL SETUP

2.1. General description of the setup

For trapping and cooling ³⁹K and ⁴⁰K the same setup was used, whose scheme is shown in Fig. 1.

The source of the atomic gas is a thermal beam. Some atoms are decelerated in the Zeeman slower, and then enter the MOT. Further in Section 2.2–2.6 the setup is described in more detail Laser radiation with frequencies near the D2 line of potassium with a wavelength of $\lambda = 766.7$ nm. Energy levels close to resonance with radiation are shown in Fig 1.

Vacuum inside the setup is maintained by two magnetodischarge pumps between the atom source and the decelerator, as well as getter and magneto-discharge pumps connected to the MOT side. Transition from ³⁹K to ⁴⁰K requires a small change in the optical scheme, which is described in Section 2.6.

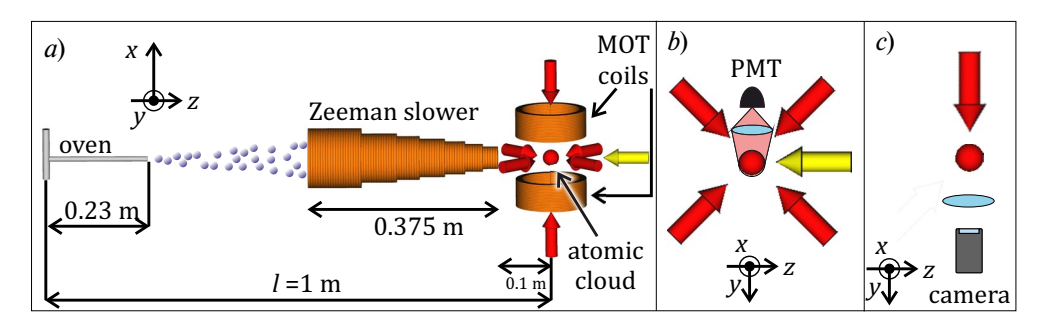


Fig. 1. (a) General view of the experimental setup for creating magneto-optical traps for ³⁹K and for ⁴⁰K. Here, "oven" is a thermal source of atoms consisting of a vertical cup and horizontal nozzle; MOT coils are MOT electromagnets; six red arrows are MOT beams; and the yellow arrow is a decelerator beam. (b) Scheme for observing fluorescence during MOT accumulation, PMT is a photomultiplier tube, the lens is shown in blue. (c) Scheme for shadow imaging of atoms, the probe beam is shown with a red arrow

2.2. Thermal atomic beam

The source of the thermal atomic beam is a stainless steel oven consisting of a vertical cup and a horizontal nozzle with an internal diameter of $2r_{\rm oven}=6.4$ mm and length 230 mm, shown in Fig. 1a. Metallic potassium is loaded into the cup. For experiments with $^{39}{\rm K}$ two glass ampoules are loaded, each containing 10 mg of natural mixture of potassium isotopes, in which $^{39}{\rm K}$ constitutes 93.2%. The ampoules are broken in the argon atmosphere, then the cup is closed from above, and the gas is pumped out. For experiments with $^{40}{\rm K}$ similarly , an ampoule containing 2.5 mg of metallic potassium enriched to 12.8% in $^{40}{\rm K}$ is broken.

To create a thermal beam ³⁹K the cup is heated to 140°C, which produces atoms with the most probable velocity of 510 m/s. The nozzle temperature along most of its length is close to room temperature. Atom deposition on the walls did not lead to any noticeable narrowing of the nozzle, with only a slight coating observed when the vacuum chamber was opened.

Atoms fly out of the nozzle at a full angle of 3.5° . Their flux can be estimated based on the saturated vapor pressure of potassium in the cup at 140° C [26], which gives $2.6 \cdot 10^{15}$ atoms/s. The MOT capture region is visible from the cup at an angle of 2° , and the decelerator output aperture cuts off atoms flying at angles exceeding 1.7° .

The pressure in the area near the furnace is $6 \cdot 10^{-8}$ Torr at the furnace temperature 140 °C measured by a magnetodischarge pump assuming that the main gas is H_2 . The actual gas composition is unknown. The potassium contribution is probably not primary since the potassium vapor pressure at room temperature, at which the walls in this area are located, is an order of magnitude lower and equals $9 \cdot 10^{-9}$ Torr. The pressure measured with the furnace heating turned off is $8 \cdot 10^{-9}$ Torr assuming the main contribution is hydrogen.

In experiments with 40 K, the cup was heated to $88-120^{\circ}$ C.

2.3. Zeeman slower

The Zeeman slower [27] allows slowing down a portion of atoms in the thermal beam and thus increasing the MOT loading rate. The slower consists of a beam counter-propagating to the atomic beam and an electromagnet with a conical winding shown in Fig. 1.

For ³⁹K, the beam is tuned to slow atoms at the transition

$$4S_{1/2}(F=2,F_z=F) \rightarrow 4P_{3/2}(F'=3,F_{z'}=F'),$$

the beam polarization σ^+ . at the trap region, the beam diameter at intensity level 1 / e equals 19 mm, and the intensity in the center is 20 mW/cm², which is much higher than the saturation intensity of the circular transition 1.75 mW/cm². At the nozzle edge, the beam diameter approximately equals the nozzle diameter. The detuning from the transition frequency is selected by maximizing the number of atoms in the MOT and equals $\Delta_0 = -11.5\Gamma$ in the zero magnetic field, where $\Gamma = 2\pi(6.035\text{MHz})$ — is the inverse lifetime of the excited state [28].

The electromagnet was originally designed for slowing 6 Li. The current magnitude is selected so that to maximize the number of atoms in the trap, and for 39 K it was 7.7 A. This value was used for the trap with the highest values of $N \simeq 7 \cdot 10^9$. Additionally, measurements were performed with a smaller number of atoms in the trap $N \simeq 5 \cdot 10^8$ at a current of 6.3 A.

The field profile on the decelerator axis at a current of 7.7 A is shown in Fig. 3a

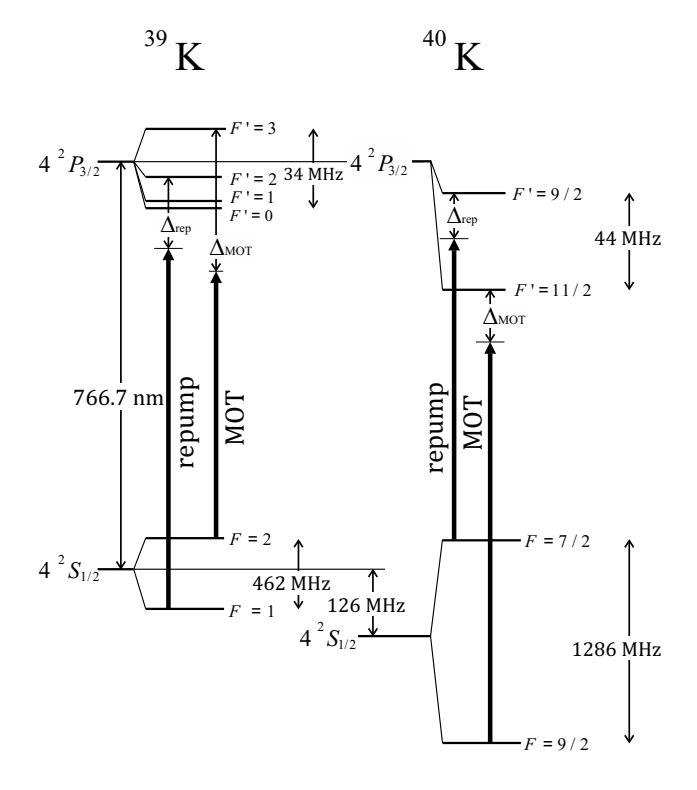


Fig. 2. Energy levels 39 K and 40 K close to resonance with radiation. Adapted from [25]

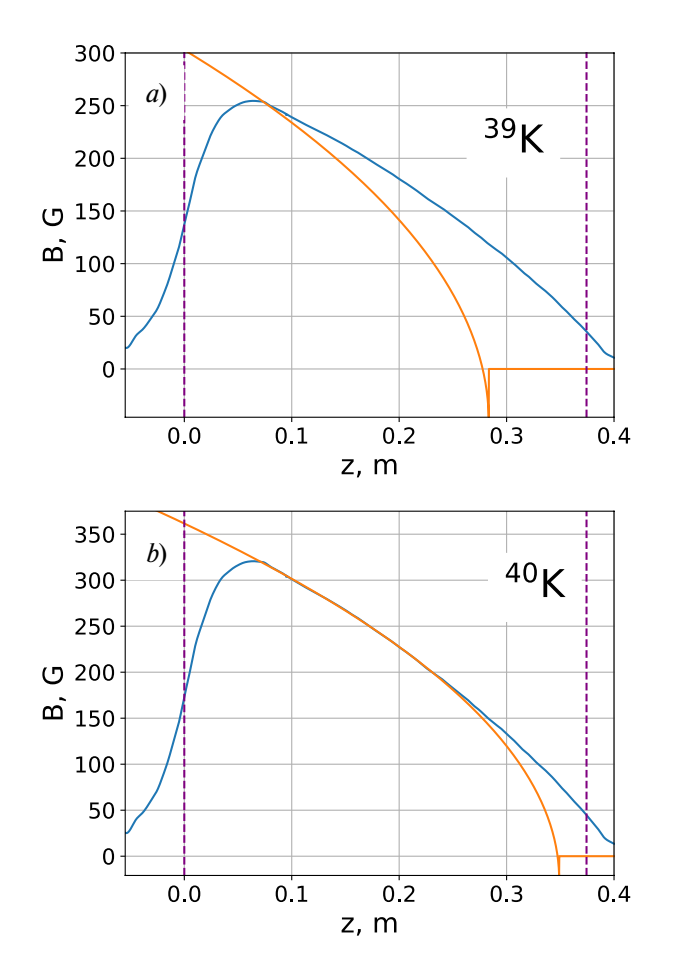


Fig. 3. Magnetic field profile along the axis of the Zeeman slower for 39 K (a) and 40 K (b). Blue stands for the measured field at 7.7 A ((a), for 39 K) and 9.7 A ((b), for 40 K), orange stands for the field of ideal decelerator (1) for given detunings Δ_0 . Vertical dashed lines show the electromagnet boundaries

The field of an ideal decelerator is also shown

$$B(z) = \frac{\hbar}{\mu_{\text{Bohr}}} \left[\Delta_0 + \frac{2\pi}{\lambda} \sqrt{2a_{\text{max}}(z_0 - z)} \right], \tag{1}$$

which corresponds to uniformly decelerated motion with the acceleration $a_{\rm max} = \pi \hbar \Gamma / (m \lambda)$, where m is the atomic mass, and $\mu_{\rm Bohr}$ — is the Bohr magneton. The actual field decreases more slowly than the ideal one, making the deceleration process more stable against abrupt magnetic field changes and light intensity reduction. The intersection of the ideal profile with the actual one in Fig. 3a corresponds to the initial velocity

$$v_{\text{ini}} = \frac{\lambda}{2\pi} \left(\frac{\mu_{\text{Bohr}} B(z = 9 \text{ cm})}{\hbar} - \Delta_0 \right) = 330 \text{ m/c,}(2)$$

which in turn corresponds to the involvement of thermal distribution of atoms in deceleration.

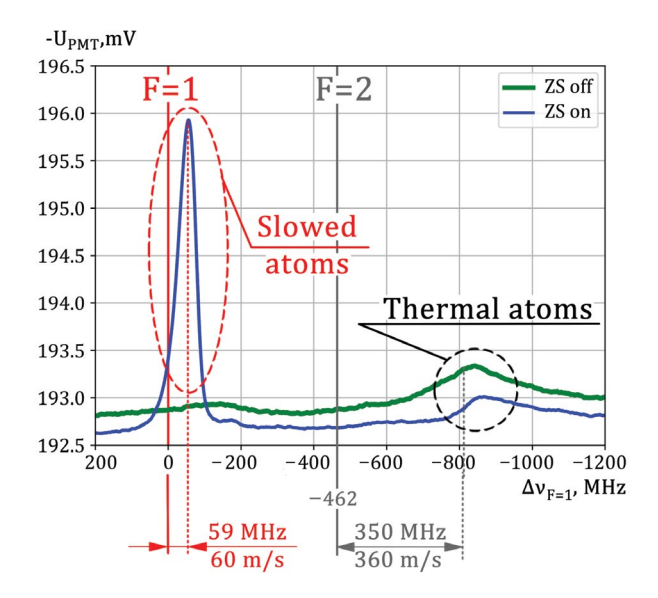


Fig. 4. Fluorescence of a beam of atoms passed through a Zeeman slower, depending on $\Delta v_{F=1}$ and the diagnostic beam detuning depending on the frequency of the transition $4S_{1/2}(F=1) \rightarrow 4$ $P_{3/2}(F'=2)$. The resonance with this transition and with 4S $_{1/2}(F=2) \rightarrow 4\,P_{3/2}(F'=3)$ is marked by the vertical lines F=1 and F=2, respectively. ZS on/off means decelerator on/off. Fluorescence is measured in units of the output voltage of the photomultiplier $U_{\rm PMT}$ and is visible against the background of illumination of the photomultiplier by over-reflections

In the MOT region, the decelerator creates a small field of about 2 G. In all experiments with MOT, this field is compensated by a coaxial electromagnet located on the other side of MOT and not shown in Fig. 1.

The effect of the decelerator can be seen in Fig. 4, which shows the fluorescence of the beam in the diagnostic beam in the area where MOT is subsequently observed.

The diagnostic beam is directed at an angle 42° to the beam axis in the plane yz, against the atomic motion. In this measurement, the MOT-creating fields are absent. The diagnostic beam diameter is 5.5 mm at the intensity level 1/e, the center intensity 0.5 mW/cm^2 , polarization is linear in the plane yz. Fluorescence is observed on a photomultiplier tube (PMT) at various detunings of the diagnostic beam $\Delta v_{F=1}$ from the transition frequency

$$4S_{1/2}(F=1) \rightarrow 4P_{3/2}(F'=2).$$

The figure shows the dependence with the decelerator turned on and off. The switching off is achieved by changing the polarization of the decelerating beam to σ^- , which has almost no

effect on the PMT illumination from rereflections, the light from which dominates over fluorescence, as seen in Fig. 4.

The slowed atoms in Fig. 4 appear near $\Delta v_{F=1} = 0$ since the slowing process for most atoms ends with pumping into the state $4S_{1/2}(F=1)$ due to the significant radial component of the magnetic field at the output of the decelerator. From the detuning of the slowed atoms peak, their longitudinal velocity can be determined as 60 m/s, which is close to the estimate $-\lambda\Delta_0$ / $(2\pi) = 54$ m/s. Unslowed atoms are mainly in the state $4S_{1/2}(F=2)$. The decay in their distribution is 350 MHz away from the resonance

$$4S_{1/2}(F=2) \rightarrow 4P_{3/2}(F'=3),$$

as noted in Fig. 4. This frequency shift corresponds to the Doppler shift for atoms with a velocity of 360 m/s, which is close to estimate (2).

For ⁴⁰K atomic deceleration on the transition was used.

$$4S_{1/2}(F=9/2, F_z=F) \rightarrow 4P_{3/2}(F'=11/2, F_{z'}=F').$$

To prevent the beam from interfering with the formation of MOT located at the beam center, in experiments with 40 K, a 6 mm diameter area at the center was darkened. Without darkening, the intensity at the center in the MOT region would be 35 mW/cm². The detuning from resonance $\Delta_0 = -5.8\Gamma$, which corresponds to a velocity of 27 m/s. The electromagnet current is 9.7 A, the number of atoms in MOT was lower by at least an order of magnitude.

The actual field profile at 9.7 A and the close profile of an ideal decelerator are shown in Fig. 3b. One can see that the actual and ideal field profiles almost coincide over a wide segment $9 \, \text{sm} < z < 25 \, \text{sm}$, with deviations in this area not exceeding 2 G. If atoms break away from the slowing process in this section, then the decelerator works fully only at $z > 25 \, \text{cm}$, where the field decreases more smoothly than in the ideal decelerator The boundary $z = 25 \, \text{cm}$ corresponds to slowing from velocities $v_{\text{ini}} = 220 \, \text{m/s}$, that is, involving only 3.6% of the thermal distribution of atoms in slowing.

For ⁴⁰K neither slowed nor thermal atoms were observed. The possibility of effective slowing with

a field profile close to ideal was confirmed by the example of ³⁹K. It was found that at 10 A current, the number of slowed atoms is approximately 30% higher than it is at 7.7 A.

2.4. Magneto-optical trap

The magneto-optical trap is formed near the exit of the Zeeman slower. The position of the trapped atomic cloud is shown in Fig. 1. The center of the trap coincides with the atomic beam axis. The trap is created by three pairs of counter-propagating beams and a pair of electromagnets with counter-flowing currents, following the traditional scheme [7]. The pressure near the MOT is $3 \cdot 10^{-10}$ Torr assuming the main gas is H_2 . The beam diameter is 18 mm at intensity level 1/e, with circular polarizations. Each beam contains two frequencies, viz. the main frequency and the repump frequency.

For ³⁹K, the main frequency component interacts with the transition

$$4S_{1/2}(F=2) \rightarrow 4P_{3/2}(F'=3),$$

shown in Fig. 2a. The detuning from the transition is $\Delta_{\text{MOT}} = -10\Gamma$, the component intensity at the center of each horizontal beam is 12.5 mW/cm², and at the center of each vertical beam it is 10 mW/cm². The repump frequency is close to the transition

$$4S_{1/2}(F=1) \rightarrow 4P_{3/2}(F'=2)$$

and detuned by $\Delta_{\rm rep} = -5\Gamma$. Due to the proximity of excited levels $4P_{3/2}(F'=3)$ and $4P_{3/2}(F'=2)$, the main frequency leads to frequent transitions to the latter and decays to $4S_{1/2}(F=1)$, which requires a sufficiently strong repump field to be depleted, with an intensity at the center of each horizontal beam of 4 mW/cm^2 , and at the center of the vertical beam of 20 mW/cm^2 . The electromagnets create a magnetic field gradient, the magnitude of which in the vertical direction x equals -9.5 G/cm. This value was used for the trap with the largest $N \simeq 7 \cdot 10^9$.

Additionally, temperature measurements for $^{39}{\rm K}$ were performed with fewer atoms $N \simeq 5 \cdot 10^8$. In these experiments $\Delta_{\rm MOT} = -6\Gamma$, $\Delta_{\rm rep} = -3\Gamma$, the magnetic field gradient was $-3.5~{\rm G/cm}$.

For trapping ⁴⁰K, the main frequency of MOT beams is close to the transition

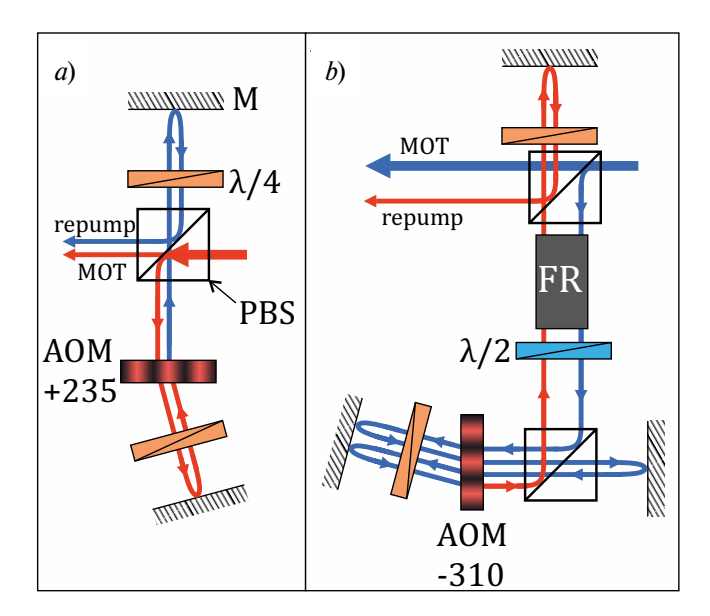


Fig. 5. Optical scheme for adding the repump frequency to the main frequency of magneto-optical trapping (MOT): (a) for 39 K; (b) for 40 K. Beams drawn close and parallel are in the same spatial mode, including MOT and repump beams. "AOM +235" and "AOM -310 MHz," are AOMs shifting the light frequency by +235 and -310 MHz respectively. PBS is the polarizing beam splitter, λ / 2 and λ / 4 are the half- and quarter-wave phase shifters, respectively, FR - Faraday rotator of polarization at 45°, and M is the mirror

$$4S_{1/2}(F = 9 / 2) \rightarrow 4P_{3/2}(F' = 11 / 2)$$

and detuned below it, $\Delta_{\text{MOT}} = -4\Gamma$. The intensity of this frequency component at the center of each horizontal and vertical beam is -5 and 10 mW/cm^2 respectively. The repump frequency component is detuned from the transition

$$4S_{1/2}(F = 7/2) \rightarrow 4P_{3/2}(F' = 9/2)$$

by $\Delta_{\rm rep} = -3.5\Gamma$. The hyperfine splitting of the level $4P_{3/2}$ is large enough, so high repump intensity is not required. In each horizontal and vertical beam, the intensity is 1.3 and 2.5 mW/cm² respectively. The vertical magnetic field gradient is -7.5 G/cm.

2.5. Camera and photomultiplier tube

The data sources are a photomultiplier tube (PMT) and a CMOS camera, whose positions are schematically shown in Fig. 1b and Fig. 1c respectively. The PMT was used to measure atom accumulation time in the MOT. The camera imaged the cloud of atoms by shadowgraphing in light with a near-resonance frequency. The PMT and camera cannot be used simultaneously. Either one or the other device is installed.

2.6. Setup modification when changing isotopes

Switching from one isotope to another requires changes in the optical scheme where the repump frequency is added to the main MOT frequency. The schemes for 39 K and 40 K are shown in Fig. 5*a* and Fig. 5*b*, respectively.

In the case of ³⁹K, the repump frequency is added to the main frequency using an acousto-optic modulator (AOM) in the double-pass mode. For ⁴⁰K, it is added by AOM in the four-pass mode.

The addition occurs before splitting the beam into three pairs of MOT beams shown in Fig. 1.

3. NUMBER AND TEMPERATURE OF ATOMS IN MAGNETO-OPTICAL TRAPS

3.1. ³⁹K

3.1.1. ³⁹K fluorescence

A photograph of atoms fluorescing in MOT beams is shown in Fig. 6a. The image was taken with a consumer digital camera, so the yellow tint of the cloud is a color reproduction error.

3.1.2. Number of ³⁹K atoms

The number of atoms was measured using shadow imaging in a monochromatic radiation field with the frequency shifted by Δ_{photo} from the transition

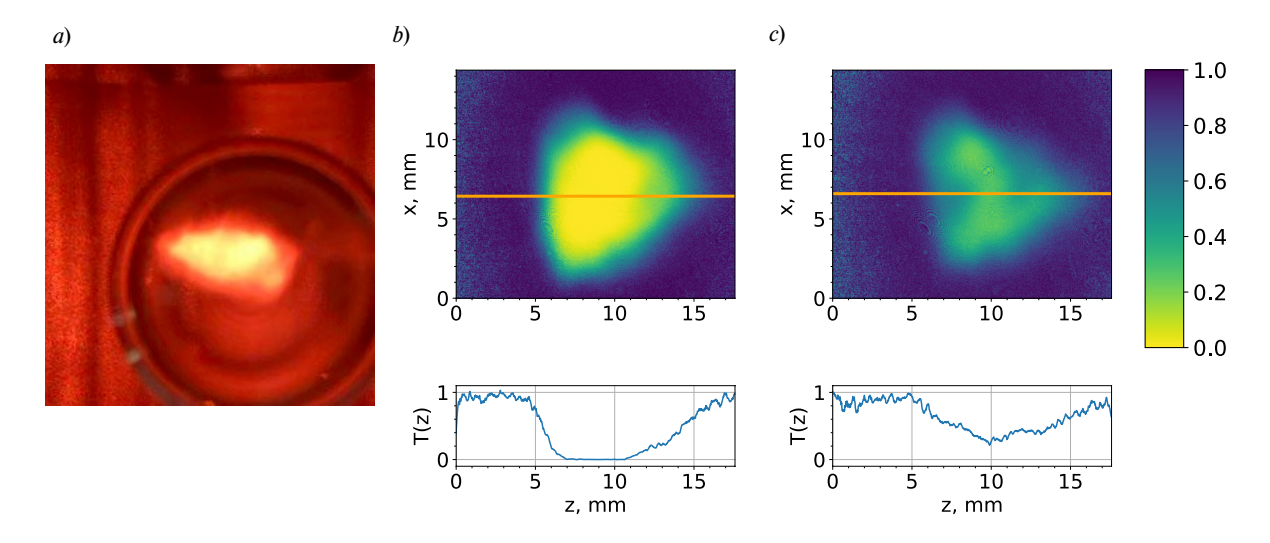


Fig. 6. (a) Fluorescence of several billion atoms 39 K in the MOT. (b), (c) Shadow images for the cloud 39 K without expansion when detuning the illuminating beam $\Delta_{\text{photo}} = -0.2\Gamma$ (b) and $\Delta_{\text{photo}} = 2.5\Gamma$ (c). The distribution of the transmission coefficient T(x,z), whose value is reflected in color, is shown. Below each image, the distribution T(x = const, z) along the orange line is shown, smoothed over the neighboring points along the line. On panel (c) the visible number of atoms $N = 8.7 \cdot 10^9$

 $4S_{1/2}(F=1) \rightarrow 4P_{3/2}(F'=2)$. Before imaging, atoms are accumulated in the trap for 40 s, with the 1/e level reached in approximately 10 s. 500 ms before imaging, the slowing beam is blocked by a mechanical shutter. 200 μ s before imaging, the MOT repump beams are switched off for 100 ns using an AOM, which transfers most atoms to the state $4S_{1/2}(F=1)$. The MOT beams are blocked by a mechanical shutter within 20 μ s. The imaging occurs at the instant of shutter closure or with a controlled delay. The magnetic fields of the MOT and decelerator remain on during imaging.

The imaging consists of turning on for 2 μ s the probe beam shown in Fig. 1c and propagating along the yaxis. The beam diameter significantly exceeds the cloud size, with central intensity of 0.24 mW/cm² \ll of saturation intensity. The atoms create a shadow in the beam. The transmitted light is projected onto the camera. By comparing images with and without the atomic cloud, one can find the transmission coefficient distribution T(x,z) used to calculate the column gas density

$$n_2(x,z) = -\frac{1}{\sigma} \ln T(x,z),$$
 (3)

where σ is the cross section of light scattering by a single atom, and the number of atoms

$$N = \int n_2(x, z) dx dz. \tag{4}$$

The image of the cloud immediately after switching off the MOT beams is shown in Fig. 6b. The cloud is elongated vertically unlike the cloud in photograph 3.1.1a due to a slight difference in MOT beam alignment. Image 6b was taken at resonance, which leads to almost complete light scattering near the cloud center and does not allow reliable calculation of $n_2(x,z)$ and N. Therefore, for quantitative analysis, images with detunings $|\Delta_{\text{photo}}| = (2.5-5.5)\Gamma$, were used, an example is shown in Fig. 6c. For such detunings σ can be calculated by summing the transition probabilities from the states $4S_{1/2}(F = 1, F_z)$ to all available levels $4P_{3/2}(F' = 0,1,2)$ and averaging over equal populations of the initial magnetic states F_z . The splitting of excited levels can be neglected, which gives

$$\sigma(\Delta_{\text{photo}}) = \frac{\lambda^2 / \pi}{1 + \left(2\Delta_{\text{photo}} / \Gamma\right)^2}.$$
 (5)

The calculation of σ is independent of polarization.

The number of particles N measured at different $\Delta_{\rm photo}$ is shown in Fig. 7.

We will take the average as an approximation of the true value. Thus, $(6.9\pm1.3)\cdot10^9$ atoms are captured in the ^{39}K trap.

In Section 3.2.2 using the example of 40 K it is shown that at the furnace temperature $> 120^{\circ}$ C

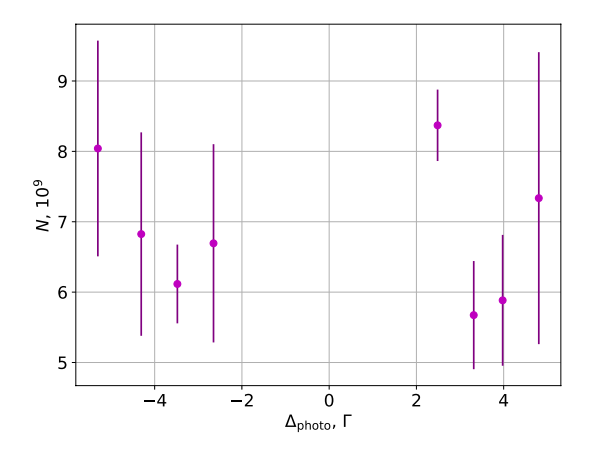


Fig. 7. Number of atoms 39 K in MOT measured using a probe beam with different detuning from resonance Δ_{photo} . Means and standard deviations for two repetitions are shown

the main limiting factor in the number of atoms is collisions with the atomic beam. As a result, shifting the MOT center beyond the atomic beam can lead to a N increase by 2 or more times.

The number of atoms can also be measured by the fluorescence of atoms in the MOT beams. We compare the two methods. In shadow imaging, it is known that almost all atoms are at a specific hyperfine level. Data interpretation requires a model that would provide the population of magnetic sublevels. Here, the model is replaced by an assumption of equal population, based on which σ (5) was calculated. Data interpretation depends on the detuning Δ_{photo} . Measurements were conducted at various Δ_{photo} , and the proximity of results indicates correct accounting for detuning. Additionally, shadow imaging also allows determining the temperature, as shown in Section 3.1.3.

Converting the number of fluorescence photons to the number of atoms depends on more parameters. A model is needed that would indicate the populations of ground and excited hyperfine levels and their magnetic states. Populations depend on the local magnetic field, intensities and detunings of the MOT bichromatic field, and spontaneous emission from surrounding atoms. Collective effects related to MOT field attenuation and photon rescattering become noticeable already at $N=10^5$ [29]. The method thus depends on calculations and assumptions to a much greater extent than shadow imaging and for this reason was not used here.

3.1.3. ³⁹K thermometry

Temperature was measured by gas expansion after switching off the MOT optical fields. Figures 8a-c show the example images of the atom concentration t = 0, 2, 4 ms after the start of expansion.

Temperature measurements were performed with a smaller number of atoms $N \simeq 5 \cdot 10^8$. Due to lower optical cloud depth, resonant radiation was use $\Delta_{\rm photo} = 0$. When calculating the scattering cross-section, only one excited level is taken into account $4P_{3/2}(F'=2)$, averaging over magnetic sublevels yields

$$\sigma = \frac{5\lambda^2}{12\pi}.\tag{6}$$

The cloud has an elongated shape in all images. Also, expansion in the long direction occurs faster. A possible reason lies in trap imbalance after switching off the repump beams, which make a significant contribution to confinement. For each image, the root-mean-square half-widths in two directions were found by fitting with a two-dimensional Gaussian profile. The sizes along the long and short directions are plotted in Figs. 9a and 9b).

The dependencies are fitted with free expansion formulas

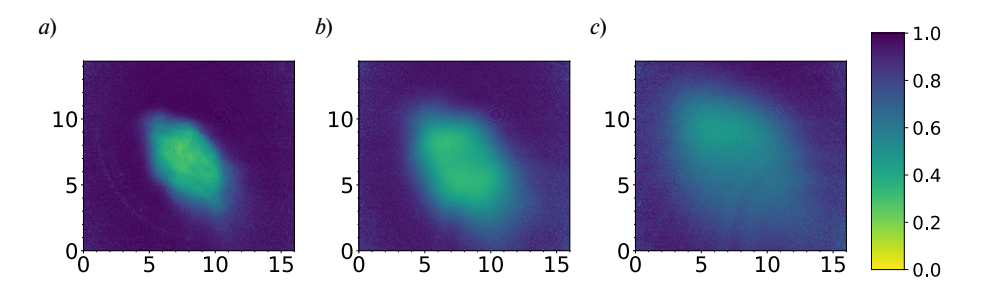


Fig. 8. Shadow images of the cloud 39 K after 0 (a), 2 (b) and 4 (c) ms after disconnecting the MOT optical fields. Coordinates are plotted in mm, and the color indicates the transmission coefficient value T(x,z)

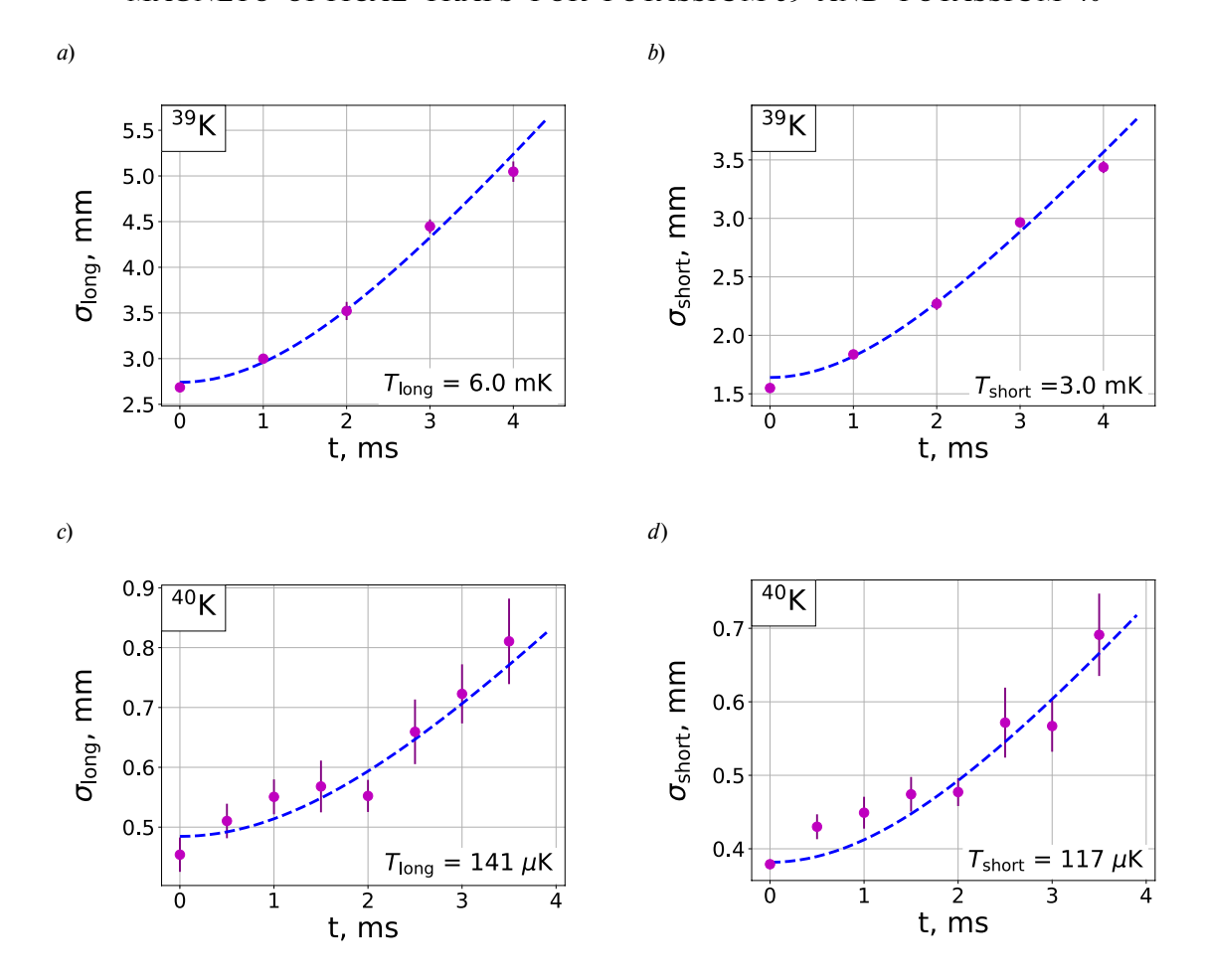


Fig. 9. Root-mean-square size of the atomic cloud depending on the expansion time t for 39 K (a, b) and 40 K (c, d). Sizes along long and short directions, σ_{long} and σ_{short} respectively, are shown. Purple dots are data, curves are fit (7), and temperatures obtained by fitting are indicated

$$\sigma_{\text{long(short)}}(t) = \sqrt{\sigma_{\text{0long(short)}}^2 + t^2 \frac{T_{\text{long(short)}}}{m}},$$
 (7)

which gives two temperature values $T_{\rm long}$, $T_{\rm short}$. As a temperature estimate, we take the average, and we take the half-difference as the systematic error, obtaining $T=4.5\pm1.5$ mK.

The obtained temperature is noticeably higher than the value $T=870~\mu\mathrm{K}$ predicted by the cooling theory of a two-level atom in a weak field [30] at $\Delta_{\mathrm{MOT}}=-6\Gamma$. In experiments [19, 31] temperatures from 2 to 6 mK were measured. Cooling ³⁹K differs from cooling of a two-level atom and from polarization gradient cooling [32]. The difference is related to the small hyperfine splitting of the excited state and the consequently increased role of repumping. For lithium isotopes, which also have small hyperfine splitting of the excited state,

temperatures from 1 to 4 mK have been reported [6, 33]. Additionally, there is a general effect of increase in T with the growth N as $(T - T_0) \sim N^{1/3}$, where T_0 is the temperature at small N [34].

3.2. 40 K 3.2.1. Number of 40 K atoms

Unlike measurements with 39 K, the repump frequency is switched off simultaneously with the main one, rather than in advance, so at the time of imaging the vast majority of atoms are in the state $4S_{1/2}(F=9/2)$. For imaging, a probe beam in resonance with the transition $4S_{1/2}(F=9/2) \rightarrow 4P_{3/2}(F'=11/2)$ is used. The scattering cross-section is obtained by averaging over equal populations of magnetic sublevels of the initial level

$$\sigma = \frac{3\lambda^2}{5\pi}.$$
 (8)

494 BATURO et al.

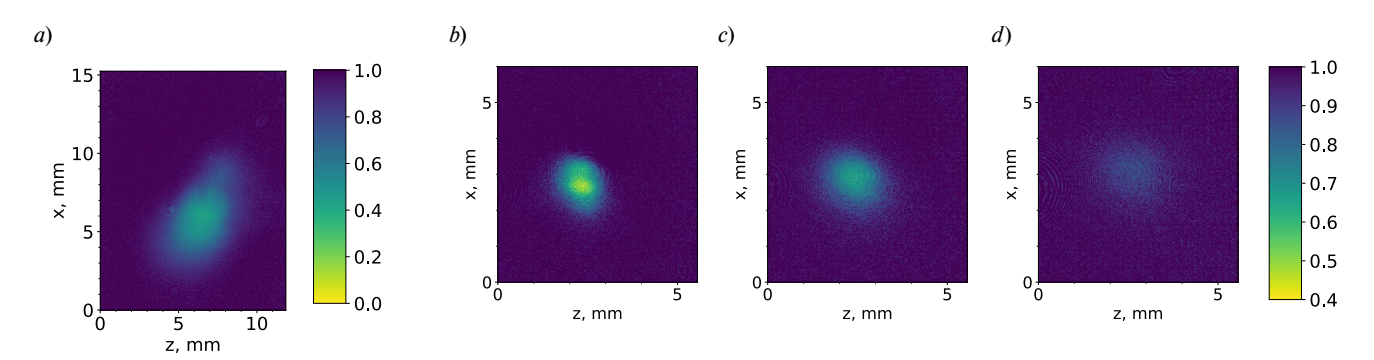


Fig. 10. Shadow images of the cloud 40 K after expansion during t = 0 (a), 0 (b), 1.5 (c), 3.5 (d) ms. Coordinates are in mm. Color shows the value of T(x,z), with the color scale for (b)-(d) differing from the scale for (a). The number of atoms $N = 1.5 \cdot 10^8$ (a), $6.3 \cdot 10^6$ (b), $7.7 \cdot 10^6$ (c), $5.5 \cdot 10^6$ (d), the measurement error for (b)-(d) is $\pm 10^6$

Shadow image of the atomic cloud immediately after switching off the optical fields of the decelerator and MOT is shown in Fig. 10a. Number of atoms in the image $N = (1.46 \pm 0.09) \cdot 10^8$. The measurement error is related to slight variations in the probe beam power between shots, including closely timed photographs with and without atoms.

The number of atoms $N=1.5\cdot 10^8$ is two orders of magnitude less than the number of atoms 39 K, although for trapping 40 K a mixture enriched up to 12% in 40 K. was used. Such enrichment suggests $\sim 10^9$ atoms 40 K in the trap since other experimental conditions are similar. The reason for the difference between actual and predicted number of atoms 40 K is unclear.

3.2.2. Effect of the thermal beam on the number of atoms ⁴⁰K in the trap

MOT is located in the path of the thermal atomic beam, whose diameter in the MOT plane equals 20 mm, and the flux is almost uniform. To understand how the beam affects the MOT, the accumulation time of atoms at the level 1/e was measured as a function of the atomic flux in the beam. The flux is regulated by the temperature of the oven cup $T_{\rm oven}$. Fig. 11 shows the dependence of accumulation time τ on temperature.

The time τ obviously decreases with the increasing flux. We compare measurements with the model. The dynamics of the number of atoms in the trap is approximately determined by the equation

$$\frac{dN}{dt} = -\Gamma_{\text{vacuum}} N - \Gamma_{\text{beam}} N + F, \qquad (9)$$

where F is the number of atoms captured in the trap per unit time, $\Gamma_{\rm vacuum}$ is the collision frequency of a trapped atom with the surrounding gas in the vacuum chamber, and $\Gamma_{\rm beam}$ is the collision frequency with atoms from the beam. The accumulation time $\tau = 1 / (\Gamma_{\rm vacuum} + \Gamma_{\rm beam})$.

Both collision frequencies can be calculated. The surrounding gas is mainly H_2 , which is related to the release of atomic hydrogen from the stainless steel vacuum chamber walls [35–37]. The collision cross-section can be found using the Landau-Lifshitz-Schiff formula [38]

$$\sigma_{K-H_2(K-K)} = 8.08 \left(\frac{C_{6,K-H_2(K-K)}}{\hbar \nu} \right)^{2/5},$$
 (10)

where $C_{6,K-H-2}(K-K)$ are Van der Waals coefficients for potassium-hydrogen (potassium-potassium) collisions, and v is the velocity of the incident particle.

$$\Gamma_{\text{vacuum}} = n_{\text{H}_2} \langle v \sigma_{\text{K}-\text{H}_2} \rangle_{T_{\text{vacuum}}},$$
 (11)

where averaging $\langle ... \rangle_{T_{\text{vacuum}}}$ is performed over the thermal distribution of the surrounding gas, and concentration n_{H_2} is known from the pressure $3 \cdot 10^{-10}$ Torr measured by the magnetodischarge pump and independent of the oven temperature.

$$\Gamma_{\text{beam}} = \frac{n_{\text{K}} \overline{v} \pi r_{\text{oven}}^2}{4\pi l^2} \sigma_{\text{K}-\text{K}}, \qquad (12)$$

where l — is the distance from the cup to the MOT (Fig. 1a), the total concentration of all potassium isotopes $n_{\rm K}(T_{\rm oven})$ is known from the dependence

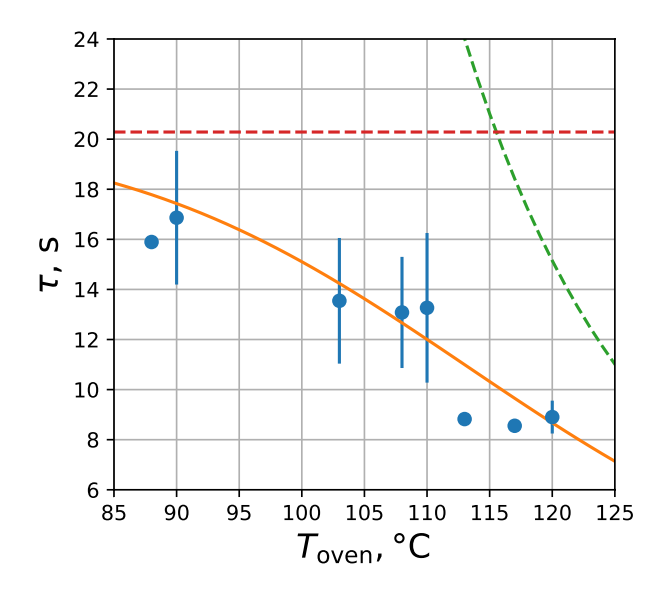


Fig. 11. Atom accumulation time in MOT depending on the oven cup temperature. Points stand for data, and solid curve stands for the calculated dependence $\tau=1/\left(\Gamma_{vacuum}+\Gamma_{beam}\right).$ Red and green dashes stand for separate contributions from $1/\Gamma_{vacuum}$ and $1/\Gamma_{beam},$ respectively

of the saturated vapor pressure on temperature [26], and \overline{v} is the thermal velocity.

The accumulation time $\tau=1/\left(\Gamma_{vacuum}+\Gamma_{beam}\right)$ calculated without fitting parameters is shown in Fig. 11 by the orange curve. This curve closely reproduces the data. The contributions Γ_{vacuum} and Γ_{beam} to the accumulation time are shown separately by dashed curves

The stationary solution of Eq. (9) gives the number of atoms in the trap $N = F\tau$. At the temperature $T_{\text{oven}} = 120^{\circ}\text{C}$ about half of the losses occur due to atoms being knocked out by the thermal beam. The shift of the trap beyond the atomic beam would allow increasing N by two times. The same method can increase the number of atoms ^{39}K . With the increasing oven temperature, the flux increases and, consequently, the possible gain from shifting the trap.

3.2.3. ⁴⁰K thermometry

The temperature of atoms in MOT was measured by gas expansion, similar to the measurement for 39 K. Figures 10b-d show images of 40 K atom concentration after t=0, 1.5, 3.5 ms from the start of expansion. It can be noticed that the cloud in Fig. 10b is significantly smaller than in Fig. 10a. Temperature measurements were performed with a depleted source, which allowed loading

 $N = (1-8) \cdot 10^6$ atoms into the trap, on average $4.4 \cdot 10^6$.

Additional processing of images 10b-d, was required as the images are less contrasting due to fewer atoms. Ring defects occurring in the image plane due to dust particles on optical surfaces can be accurately excluded only if their position is identical on the images with and without atoms. However, defects shift from image to image due to air currents and vibrations, resulting in potentially overestimated atom numbers and distorted cloud sizes in low-contrast images. The distortion prevents size determination for half of the images at t > 3ms. To suppress such errors, all shadow images used for ⁴⁰K thermometry were processed using the principal component method [39-41]. Based on seven images without atoms, a basis of four principal components was created, whose combination was used to suppress defects. Figs. 10b-d show images after processing.

The evolution of cloud sizes during expansion is shown in Figs. 9c and 9d. Unlike 39 K, the expansion anisotropy is almost absent. Temperatures for the major and minor axes were 141 μ K and 117 μ K, respectively. Based on the average and spread of these values, we obtain a temperature of $T=129\pm12$ which is 35 times lower than the temperature of 39 K.

Temperature of ^{40}K was found to be below the Letokhov-Minogin-Pavlik limit $\hbar\Gamma$ / $2=144~\mu K$ [30]. Moreover, at detuning $\Delta_{MOT}=-4\Gamma$, the cooling theory of a two-level atom in weak light [30] predicts a temperature of 590 μK . The MOT magnetic field, which remains on during expansion, has no noticeable effect on the expansion and cannot explain the difference with the two-level atom theory. A similar deviation from the two-level model was previously observed for ^{40}K in [16], where the temperature was estimated at 50 μK at detuning $\Delta_{MOT}=-3\Gamma$.

The low temperature is associated with cooling in the polarization gradient [42]. The effectiveness of such mechanism depends on the position of hyperfine levels nearest to the excited level with angular momentum F' involved in the main MOT transition [32]. For Cs, level F'-1 lies below F' by 251 MHz, and for ⁸⁷Rb it is by 266 MHz, which is much larger than typical MOT detunings Δ_{MOT} . As a result, for Cs and ⁸⁷Rb in MOT, temperatures of about 50 μ K were obtained [43, 44], three times

lower than the limit $\hbar\Gamma/2$. For 40 K, the splitting is smaller, 44 MHz, however, the level F'-1 lies above F' and therefore further from the resonance with the main MOT frequency, which again favors cooling in the polarization gradient.

4. CONCLUSIONS

Magneto-optical traps were created for 39 K and for 40 K, loaded from a Zeeman slower. Transition between isotopes is achieved by minor modification of the setup. The number of trapped atoms, $7 \cdot 10^9$ and $1.5 \cdot 10^8$, is the largest among traps, where 39 K and 40 K are loaded from the slower, respectively. For 40 K, the influence of collisions with the beam atoms on accumulation time was studied for the first time. A method for increasing the number of atoms is proposed. The measured gas temperature 39 K equals 4.5 mK. The gas temperature 40 K turned out to be much lower, about 130 μ K, which is below the Letokhov-Minogin-Pavlik limit

FUNDING

The work was supported by the Rosatom State Corporation within the framework of Quantum Computing roadmap.

REFERENCES

- 1. V. I. Balykin, V. G. Minogin, and V. S. Letokhov, Rep. Progr. Phys. **63**, 1429 (2000).
- 2. R. Onofrio, UFN 186, 1229 (2016).
- 3. C. D'Errico, M. Zaccanti, M. Fattori, G. Roati, M. Inguscio, G. Modugno, and A. Simoni, New J. Phys. 9, 223 (2007).
- **4**. T. Berrada, S. van Frank, R. Bucker, T. Schumm, J.-F. Schaff, and J. Schmiedmayer, Nat. Commun. **4**, 2077 (2013).
- A. K. Fedorov, V. I. Yudson, and G. V. Shlyapnikov, Phys. Rev. A 95, 043615 (2017).
- **6**. V. A. Vinogradov, K. A. Karpov, S. S. Lukashov, A. V. Turlapov, QE **50**, 520 (2020).
- 7. E. L. Raab, M. Prentiss, A. Cable, S. Chu, and D. E. Pritchard, Phys. Rev. Lett. **59**, 2631 (1987).
- **8**. C. Monroe, W. Swann, H. Robinson, and C. Wieman, Phys. Rev. Lett. **65**, 1571 (1990).
- 9. S. Weyers, E. Aucouturier, C. Valentin, and N. Dimarcq, Opt. Commun. 143, 30 (1997).
- **10**. A. Camara, R. Kaiser, and G. Labeyrie, Phys. Rev. A **90**, 063404 (2014).

- 11. E. Pedrozo-Pe nafiel, F. Vivanco, P. Castilho, R. R. Paiva, K. M. Farias, and V. S. Bagnato, Laser Phys. Lett. 13, 065501 (2016).
- 12. B. S. Marangoni, C. R. Menegatti, and L. G. Marcassa, J. Phys. B: Atom. Molec. Opt. Phys. 45, 175301 (2012).
- **13**. R. S. Williamson and T. Walker, J. Opt. Soc. Amer. B **12**, 1393 (1995).
- **14.** L. De Sarlo, P. Maioli, G. Barontini, J. Catani, F. Minardi, and M. Inguscio, Phys. Rev. A **75**, 022715 (2007).
- 15. E. Wille, Preparation of an Optically Trapped Fermi-Fermi Mixture of 6Li and 40K Atoms and Characterization of the Interspecies Interactions by Feshbach Spectroscopy, PhD thesis, University of Innsbruck, Innsbruck (2009).
- F. S. Cataliotti, E. A. Cornell, C. Fort, M. Inguscio, F. Marin, M. Prevedelli, L. Ricci, and G. M. Tino, Phys. Rev. A 57, 1136 (1998).
- 17. C. Ospelkaus, S. Ospelkaus, K. Sengstock, and K. Bongs, Phys. Rev. Lett. 96, 020401 (2006).
- **18**. M. Landini, S. Roy, L. Carcagní, D. Trypogeorgos, M. Fattori, M. Inguscio, and G. Modugno, Phys. Rev. A **84**, 043432 (2011).
- **19**. M. Landini, *A tunable Bose-Einstein condensate for quantum interferometry*, PhD thesis, Università di Trento, Trento (2011).
- A. Ridinger, S. Chaudhuri, T. Salez, U. Eismann,
 D. R. Fernandes, K. Magalhães, D. Wilkowski, C. Salomon, and F. Chevy, Eur. Phys. J. D 65, 223 (2011).
- 21. M. Prevedelli, F. S. Cataliotti, E. A. Cornell, J. R. Ensher, C. Fort, L. Ricci, G. M. Tino, and M. Inguscio, Phys. Rev. A 59, 886 (1999).
- **22**. B. DeMarco, H. Rohner, and D. S. Jin, Rev. Sci. Instrum. **70**, 1967 (1999).
- 23. Z. Lasner, D. Mitra, M. Hiradfar, B. Augenbraun, L. Cheuk, E. Lee, S. Prabhu, and J. Doyle, Phys. Rev. A 104, 063305 (2021).
- **24**. C.-H. Wu, I. Santiago, J. W. Park, P. Ahmadi, and M. W. Zwierlein, Phys. Rev. A **84**, 011601 (2011).
- 25. M. Allegrini, E. Arimondo, and L. A. Orozco, J. Phys. Chem. Reference Data, 51, 043102 (2022).
- **26**. C. B. Alcock, V. P. Itkin, and M. K. Horrigan, Canadian Metallurgical Quarterly, **23**, 309 (1984).
- **27**. W. D. Phillips and H. Metcalf, Phys. Rev. Lett. **48**, 596 (1982).
- **28**. H. Wang, P. L. Gould, and W. C. Stwalley, J. Chem. Phys. **106**, 7899 (1997).
- C. G. Townsend, N. H. Edwards, C. J. Cooper, K. P. Zetie, C. J. Foot, A. M. Steane, P. Szriftgiser, H. Perrin, and J. Dalibard, Phys. Rev. A 52, 1423 (1995).

- . V.S. Letokhov, V.G. Minogin, B.D. Pavlik, JETP **72**, 1328 (1977).
- . V. Gokhroo, G. Rajalakshmi, R. K. Easwaran, and C. S. Unnikrishnan, J. Phys. B: At. Mol. Opt. Phys. **44**, 115307 (2011).
- . A. Bambini and A. Agresti, Phys. Rev. A **56**, 3040 (1997).
- 33. S. A. Saakyan, Dissertation: Experimental studies of the properties of gas of ultracold highly excited and partially ionized lithium-7 atoms, Ph.D. in Physics and Mathematics, JIHT RAS, Moscow (2016).
- **34.** C. J. Cooper, G. Hillenbrand, J. Rink, C. G. Townsend, K. Zetie, and C. J. Foot, Europhys. Lett. **28**, 397 (1994).
- . S.-S. Hong, Y.-H. Shin, and I. Arakawa, Meas. Sci. Technol. **15**, 359 (2004).
- . J. R. J. Bennett, S. Hughes, R. J. Elsey, and T. P. Parry, Vacuum **73**, 149 (2004).
- . S. S. Hong, Y. H. Shin, and J. T. Kim, Measurement **41**, 1026 (2008).

- . L. D. Landau, E. M. Lifshitz, *Quantum Mechanics* (*Non-relativistic Theory*), Nauka, Moscow (1989), §127, p. 608.
- . K. Pearson, London Edinburgh Philos. Mag. and J. Sci. **2**, 559 (1901).
- . X. Li, M. Ke, B. Yan, and Y. Wang, Chin. Opt. Lett. **5**, 128 (2007).
- **41**. L. Krinner, *Exploring Spontaneous Emission Phenomena using Ultracold Atomic Matter Waves*, PhD thesis, Stony Brook University, Stony Brook (2018).
- . J. Dalibard and C. Cohen-Tannoudji, J. Opt. Soc. Amer. B **6**, 2023 (1989).
- . M. Drewsen, Ph. Laurent, A. Nadir, G. Santarelli, A. Clairon, Y. Castin, D. Grison, and C. Salomon, Appl. Phys. B **59**, 283 (1994).
- . H. Crepaz, *Trapping and Cooling Rubidium Atoms for Quantum Information*, PhD thesis, University of Innsbruck, Innsbruck (2006). Progr. Phys. **63**, 1429 (2000).